Article

Shake Table Test of Long Span Cable-Stayed Bridge Subjected to Near-Fault Ground Motions Considering Velocity Pulse Effect and Non-Uniform Excitation

Chao Zhang [1,2,*], **Guanghui Fu** [1], **Zhichao Lai** [1], **Xiuli Du** [2], **Piguang Wang** [2], **Huihui Dong** [2] **and Hongyu Jia** [3]

1   College of Civil Engineering, Fuzhou University, Fuzhou 350108, China; kuangjuanzhe@163.com (G.F.); laiz@fzu.edu.cn (Z.L.)
2   Key Laboratory of Urban Security & Disaster Engineering of MOE, Beijing University of Technology, Beijing 100124, China; duxiuli@bjut.edu.cn (X.D.); wangpiguang1985@126.com (P.W.); donghuihui.123@163.com (H.D.)
3   School of Civil Engineering, Southwest Jiaotong University, Chengdu 610031, China; Hongyu1016@swjtu.edu.cn
*   Correspondence: zhangchao1985@fzu.edu.cn

check for updates

Featured Application: The research conclusion on the velocity impulse effect and non-uniform excitation in this paper can be used to guide the seismic design of cable-stayed bridges.

Abstract: This paper presents the results of shake table tests of a scaled long span cable-stayed bridge (CSB). The design principles of the scaled CSB are first introduced. The first six in-plane modes are then identified by the stochastic subspace identification (SSI) method. Furthermore, shake table tests of the CSB subjected to the non-pulse near-field (NNF) and velocity-pulse near-fault (PNF) ground motions are carried out. The tests indicated that: (1) the responses under longitudinal uniform excitation are mainly contributed by antisymmetric modes; (2) the maximum displacement of the tower occurs on the tower top node, the maximum acceleration response of the tower occurs on the middle cross beam, and the maximum bending moment of the tower occurs on the bottom section; (3) the deformation of the tower and girder subjected to uniform excitation is not always larger than that subjected to non-uniform excitation, and therefore the non-uniform case should be considered in the seismic design of CSBs.

Keywords: shake table test; cable-stayed bridge; near-fault motion; velocity pulse; non-uniform excitation

1. Introduction

For a long time, the cable-stayed bridge (CSB) has been the main bridge type scheme for long-span bridges. Among them, many CSBs are located in earthquake-prone zones. Owing to their flexibility and slenderness, CSB can dissipate a major portion of the earthquake forces [1]. However, when suffering from strong earthquakes, CSBs experience large displacements and internal forces [2]. For example, the tower of Chilu bridge was seriously damaged during the CHICHI earthquake in 1999 [3]. As transportations hubs, any damage to a bridge during an earthquake may lead to serious problems.

To reveal the seismic response of long span CSBs, many studies have been carried out. Xu and Duan discussed the seismic design strategy of CSBs subjected to strong ground motion [4]. Yi and Li studied the seismic-induced bearing uplift of CSBs subjected to strong ground motions [5]. Bayraktar et al.

carried out the static and dynamic field load test on the long span Nissibi CSB. Fang et al. designed a 1/100 physical model of the Wuhan Yangtze River Bridge (three-tower CSB) and conducted a shake table test of it [6]. Seplikayadi et al. studied the seismic response of a floating CSB under earthquake excitation using a shake table test [7]. Xu et al. carried out a shake table test of a half-bridge scale model to study the longitudinal seismic responses [8]. Xie et al. designed a 1/70-scale bridge model of a super long-span CSB with a central span of 1400 m. The dynamic characteristics and seismic responses of the full bridge model with and without inelastic tower links were tested [9].

Since the length of long-span CSBs is comparable to the seismic wavelength, it is intuitively clear that all supports should be excited by the non-uniform motions [10]. Shiravand and Parvanehro studied the seismic response of CSBs under non-uniform and uniform excitations [11]. It found that the cable axial force and pylons shear were amplified up to 1.4 and 1.48, respectively. Li et al. analyzed the seismic response of a super-long span CSB induced by ground motions in different sites considering soil-structure interaction [12]. Liang et al. studied the seismic response of pile groups supporting long-span CSB subjected to multi-support excitations using shake table tests [13].

Near-fault (NF) ground motions usually caused more damages to structures [14,15]. Therefore, more attention has been given to the damage induced by NF ground motions. Seyed et al. found that significant residual displacements can be caused by NF ground motions [16]. Adanur et al. found that suspension bridges experienced higher displacements and internal forces when subjected to NF ground motions [17]. The main reason is the high velocity pulse [18]. The velocity pulse contains a great amount of energy that is expected to be imposed on the structure in a very short time interval and causes severe damage in the structure [19].

As mentioned before, NF ground motions has a great influence on the seismic performance of CSBs. In particular, the effect of velocity pulse is very significant. However, so far, the influence of NF ground motions on CSB are mostly studied by numerical methods, while the shake table tests are limited. In this paper, shake table tests on a 1/100 scale CSB with a main span of 680 m was carried out. The design, construction, instrumentation, and loading protocol of the test model were described. Furthermore, the seismic performances when suffered from uniform and non-uniform NF ground motions were tested and discussed.

2. Prototype Bridge and the Scaled Model

2.1. Prototype Bridge

The prototype bridge is a CSB with double towers located in Fuzhou (China). Figure 1 is the elevation view of the prototype bridge. The total length of the bridge is 1280 m, and the maximum span is 680 m.

The bridge consists of two concrete towers, double-plane fan-type cables, and steel box girders. The towers have a rhombus shape with a height of 220 m. Three parts of the tower (i.e., bottom, middle and top sections) have the heights of 48.6 m, 98 m and 67.4 m, respectively. The towers consist of hollow thin-walled box sections with variable dimensions. Five critical sections of the towers are shown in Figure 1b. All stayed cables are composed of numbers of high-strength strands. These strands have an elastic modulus of 175 GPa, yield stress of 1500 MPa and tensile strength of 1860 MPa. The steel box girder is made of steel with a yield stress of 370 MPa. It has a width of 30.6 m and a depth of 3.5 m, as shown in Figure 1c.
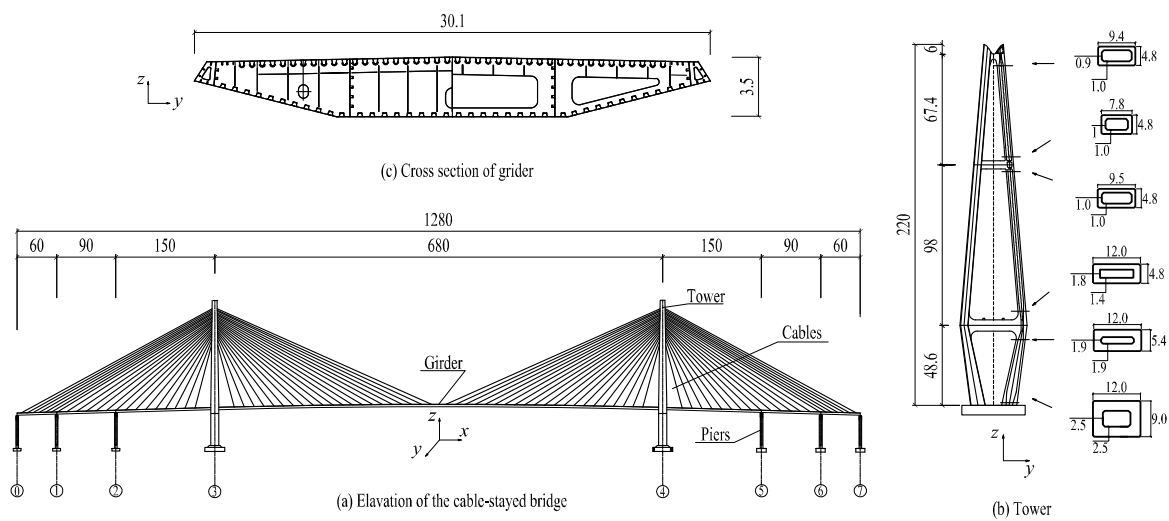
Figure 1. (**a**) Elevation of the CSB; (**b**) the cross section of girder; (**c**) the main tower.

2.2. Scaled Model

2.2.1. Shake Table System

This test is carried out on the shake tables system of Fuzhou University (China), shown in Figure 2. The shake tables system is capable of 3-freedom motions with maximum acceleration is up to 1.5 g. The effective operation frequency band is 0.1–50 Hz. The shake tables system consists of one middle tables and two side tables. The middle table is 4 m × 4 m, while the side table is 2.5 m × 2.5 m. The maximum payload of middle table and side table are 25 t and 10 t respectively. The two side tables are movable in longitudinal direction with the maximum length of 24 m. All three tables can work together or independently, which can simulate uniform excitation and non-uniform excitation separately. Other parameters of the shake tables of Fuzhou University are listed in Table 1.
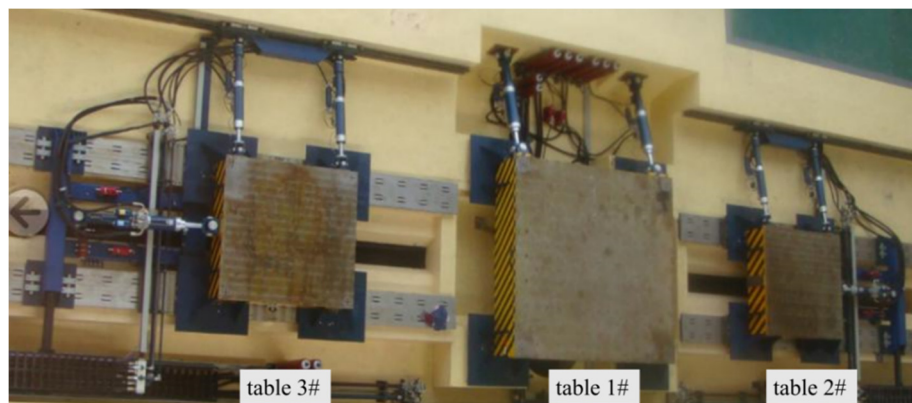

Figure 2. Shake tables system of Fuzhou University.

Table 1. Performance specifications of the shake tables system.

Table NO.	Table Size	Self-Weight	Payload	Degree of Freedom	Stroke Length	Velocity	Acceleration	Operation Frequency
1#	4 m × 4 m	9.65 t	22 t	3	±250 mm	75 cm/s	1.5 g(Ux)/1.2 g(Uy)	0.1–50 Hz
2# (3#)	2.5 × 2.5 m	3.0 t	10 t	3	±250 mm	150 cm/s	1.5 g(Ux)/1.2 g(Uy)	0.1–50 Hz

2.2.2. Similitude Ratio

For the test bridge, the towers and piers are made of polymethyl methacrylate (PMMA), as that is easy to be fabricated. The cross-sections of towers and piers are designed strictly following the geometric scaling factors of 1/100. Figure 3 shows the elaborated tower and pier.
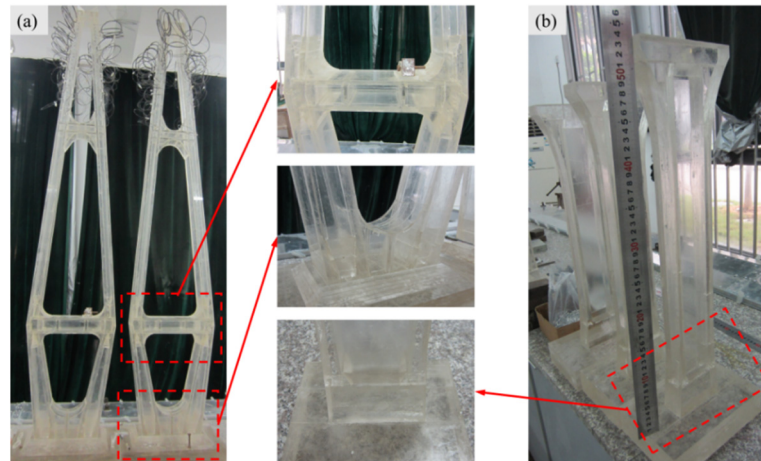

Figure 3. Detailed design of testing specimen (**a**) towers and (**b**) piers.

As the towers is the most important components of CSB, the similitude ratios of the whole CSB are determined according to tower. Based on the Buckingham theorem of dimensional analysis [20], the similitude ratios of other parameters were calculated, shown in Table 2. All other components of the test CSB are designed based on the similitude ratios in the table.

Table 2. Similitude ratios of the scale bridge model.

Physical Properties	1/Ratio	Material Properties	1/Ratio	Dynamic Parameter	1/Ratio
Length	1/102	Elastic Modulus	1/12.81	time	0.0707
Area	1/104	bending Stiffness	$1/1.281 \times 10^9$	Frequency	1/0.0707
Moment of inertia	1/108	Equivalent density	1/0.2562	Velocity	1/7.07
Strain	1	Mass	1/256,200	Acceleration	2

2.2.3. Girder and Stayed Cables

In the prototype bridge, the deck is flat, thin walled steel box with many U shape shear key. It would be very difficult to manufacture the deck if the cross-section were scaled in ratio of 1/100 stickily. Therefore, it is simply designed according similitude ratios of bending stiffness in Table 2.

The aluminum is selected as the material of girder for the characteristics of low elastics modulus, simply processed and installed. Figure 4 shows the size, area and moment of inertia of the cross section. The section stiffness EI_z and EI_z are calculated as 4.72e-06 m^4 and 1.50e-07 m^4. The actual bending stiffness ratios of EI_z and EI_z are 6.91E+08 and 5.00E+08. They are about 1.86 times and 2.56 times of target similitude ratios of bending stiffness in the Table 2.
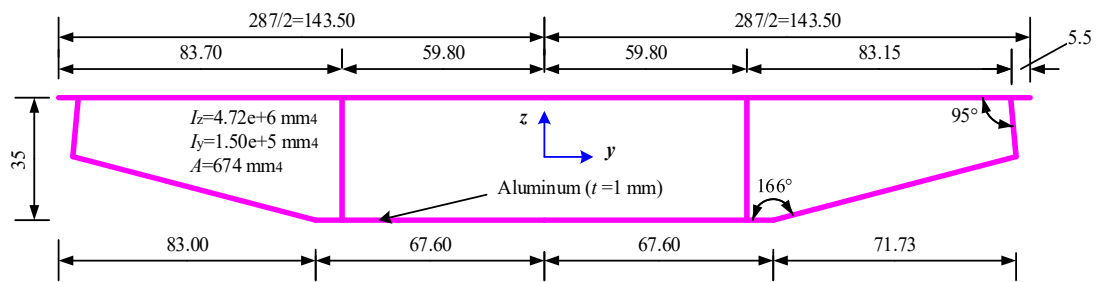
Figure 4. Simplified cross section of girder (units: mm).

The high-strength steel wire was used to fabricate stayed cables. The diameters of cables were calculated strictly followed similitude ratio of axial stiffness in Table 2. In the model, diameters of the steel wires are 0.4 mm for C1-C8, 0.6 mm for C9-C14 and 0.9 mm for C15-C21. Material tests of the polymethyl methacrylate (PMMA) and other materials were conducted, and the average properties are shown in Table 3.

Table 3. Material properties of test model.

Component	Material	Young's Modulus of Elastic E (MPa)	Density (kg/m^3)	Poisson's Ratio	Yield Strength (MPa)
tower/pier	PMMA	2.69×10^3	1180	0.391	126
girder	Aluminum	7.53×10^4	2700	0.326	187
stayed cable	Steel	1.95×10^5	7850	0.3	1330

#0, #1, #2 piers and #3 tower were placed on the middle-table (table 1#), and #4 tower, #5, #6 and #7 piers were placed on the right-side table (table 2#). All the towers and piers were fixed on the tables by high stress bolts.

Figure 5c shows the elaborate roll bearings installed between the tower and girder. The bearings can roll freely in longitudinal direction, but is restrained in the lateral direction.

Figure 5. Assembling of the components (**a**) cable anchor; (**b**) fixed tower foundation platform; (**c**) sliding bearing.

2.2.4. Additional Masses

The additional mass is calculated according to the similitude ratio of mass in table 2. In order maintain the rigidity of the bridge, the additional mass is realized by a series of discrete mass blocks. Steel blocks of different weights were prefabricated, such as 1 kg and 0.5 kg. For each tower, steel blocks with a total weight of 294 kg are fixed, shown in Figure 6a. For each pier, steel blocks with a total weight of 66 kg are fixed, shown in Figure 6b. For girder, steel blocks with a total weight of 114 kg are fixed on the deck, shown in Figure 6c.
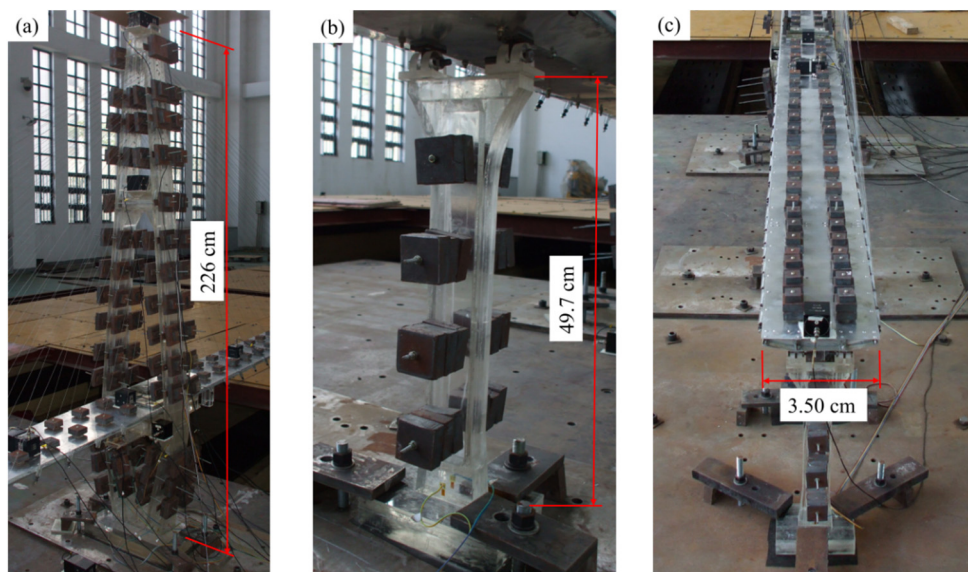
Figure 6. Arrangement of steel blocks for (**a**) tower; (**b**) pier and (**c**) girder.

2.2.5. Sensors Arrangement

The responses of the bridge model were measured by 128 channels transducers collecting (made by Dewetron Co., Grambach, Austria) with a sampling frequency of 512 Hz. The displacements and accelerations for the decks, towers, and piers were measured by two displacement transducers and 23 accelerometers, respectively. The strains in the towers and piers were measured by 54 strain gauges, which were stacked on the surface of the critical sections, such as the bottom sections of the towers and piers. Figure 7 shows all the sensors arrangement.
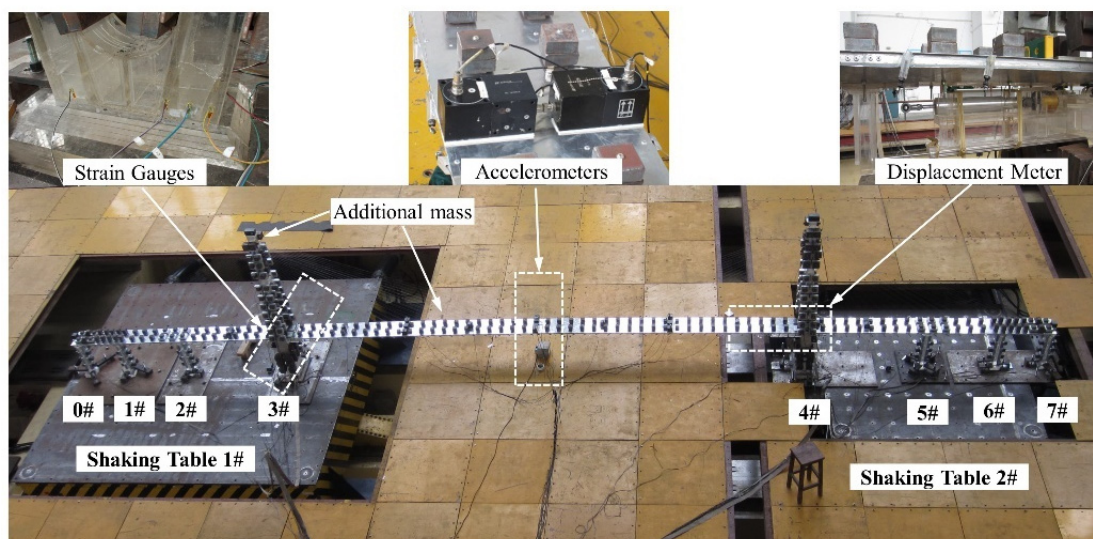

Figure 7. Bridge model assembled on shake tables.

3. Dynamic Characteristics and Test Cases

3.1. Dynamic Characteristics of the Test CSB

White noise excitation with bandwidth of 0.1~50 Hz was used to excite the dynamic characteristics of test CSB. The stochastic subspace identification method (SSI) [21] is used to identify the stochastic state space model from the recorded accelerations. Figure 8 shows the estimated in-plane modal shapes and frequencies of first six modes. The first mode is dominated by longitudinal sway of the

girder. The 2nd mode shows vertical antisymmetric vibration of girder combining longitudinal bending vibration of tower. The 2nd, 4th and 6th modes are antisymmetric around the vertical axis, while the 3rd and 5th modes are symmetric.
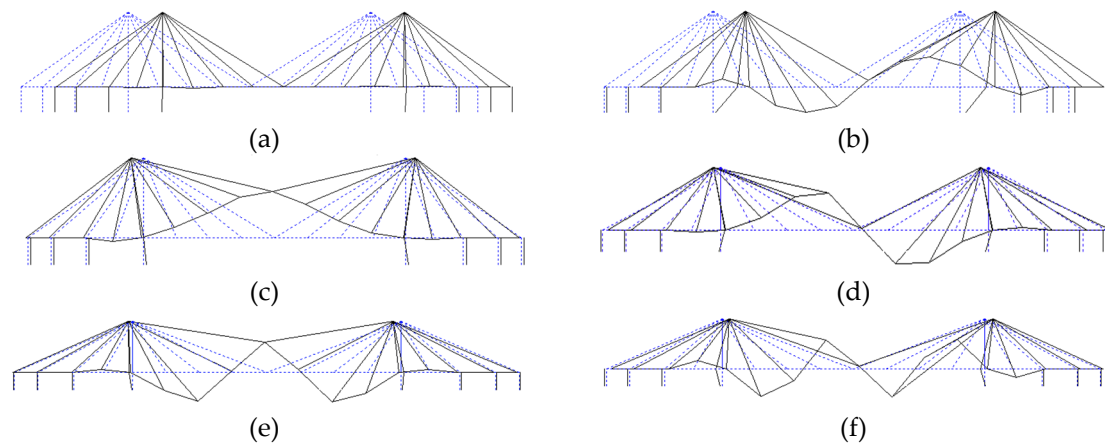
Figure 8. Identified modal shapes and frequencies (**a**) the 1st mode, f_{v1} = 0.79 Hz; (**b**) the 2nd mode, f_{v2} = 6.61 Hz; (**c**) the 3rd mode, f_{v3} = 9.34 Hz; (**d**) the 4th mode, f_{v4} = 14.19 Hz; (**e**) the 5th mode, f_{v5} = 20.97 Hz; (**f**) the 6th mode, f_{v6} = 27.16 Hz.
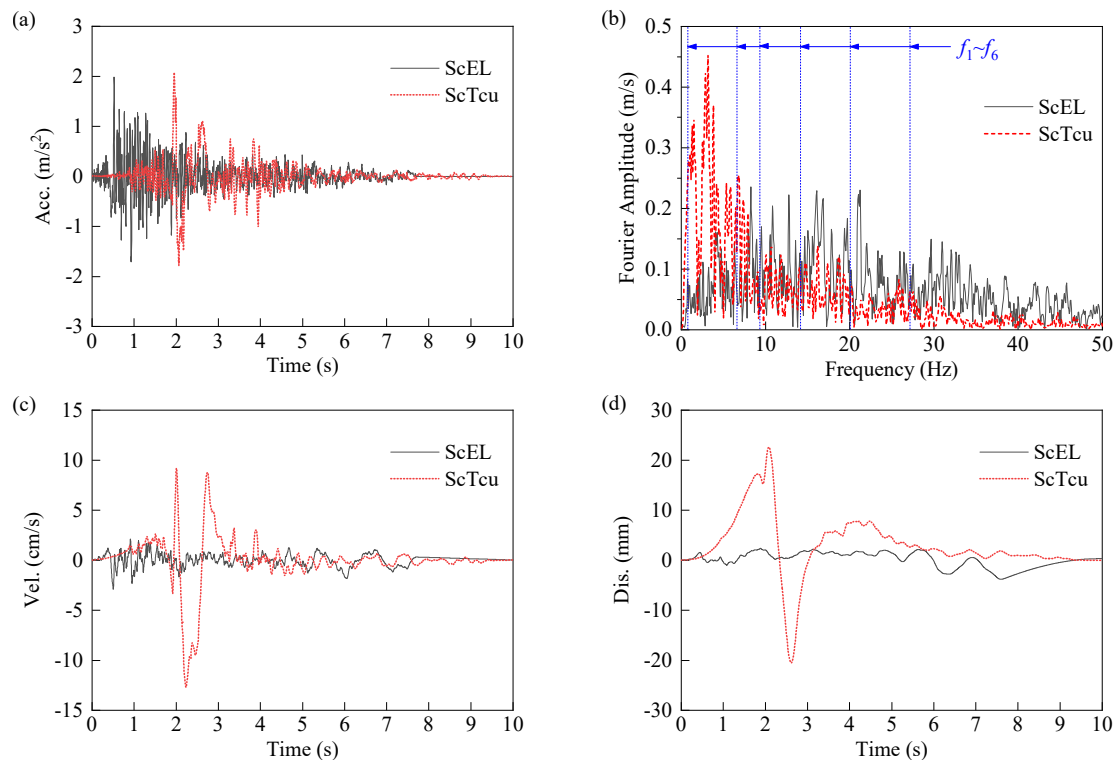
3.2. Input Ground Motions

In this paper, two near fault (NF) ground motions, recorded at stations within 20 km of the fault, are selected as input motions. The first one is EL-Centro wave, recorded in El Centro Array #9 station with epicentral distance of 6.09 km during the Imperial Valley earthquake in 1940. The ratio of PGV/PGA is 0.11. The other motion is recorded at station TCU052 with an epicentral distance of 1.84 km during the 1999 CHICHI earthquake. The PGV/PGA ratio is 0.43.

The algorithm proposed by Shahi and Baker [22] can identify pulses at arbitrary orientations. The procedure has been widely used to classify ground motions in the Next Generation Attenuation-West2 database [23]. Based on the above method, TCU052 is identified by an obvious velocity pulse, while the El-Centro motion has no velocity pulse.

During the shake table test, the PGA of both recorders are adjusted to 2.08 m/s^2. According to the similitude ratio of time in Table 2, the recorder motions are scaled in time domain. The adjusted El-Centro wave and TCU052 wave are renamed as ScEL and ScTCU respectively.

Figure 9a shows the acceleration time history of two motions. Figure 9b shows the acceleration Fourier amplitudes spectrum. It can be seen that the ScEL has more energy in the frequency range of [10 Hz, 20 Hz], while the ScTCU has higher energy in the low frequency band of f < 10 Hz. For comparison, the identified frequencies of the first six modes are marked in Figure 9b. It is obvious that the frequencies of the first two modes are close to the predominant frequency of the ScTCU.

Figure 9c,d show the velocity and displacement time histories of two motions. It shows the ScTCU has significant higher velocity than ScEL (2.89 cm/s). Besides, the maximum displacement value of ScTCU is much larger than ScEL, shown in Figure 9d. In conclusion, the ScTCU is stand for the PNF ground motion, while the ScEL can be seen as NNF ground motion.

Figure 9. Input ground motions (**a**) Acceleration time histories; (**b**) Acceleration Fourier Amplitude; (**c**) Velocity time histories; (**d**) Displacement time histories;

3.3. Shake Table Test Cases

When subjected to longitudinal earthquakes, CSBs respond to the significant internal force of the tower and large displacement of the girder [24]. It is usually one of the control cases of the seismic design of cable-stayed bridges [25]. Although lateral and vertical ground motions will also have a non-negligible effect on the seismic response of the CSB. However, when considering multi-directional seismic excitation, the seismic responses of the CSB are more complicate as multi-directional excitations maybe coupled. It is unfavorable to study the influence law of velocity pulse effect or wave passage effect. In order to avoid the complexity caused by multi-directional seismic excitations, this experiments only focuses on seismic responses of CSB subjected to longitudinal seismic excitation. The schematic diagram of input excitations and sensors are shown in Figure 10.
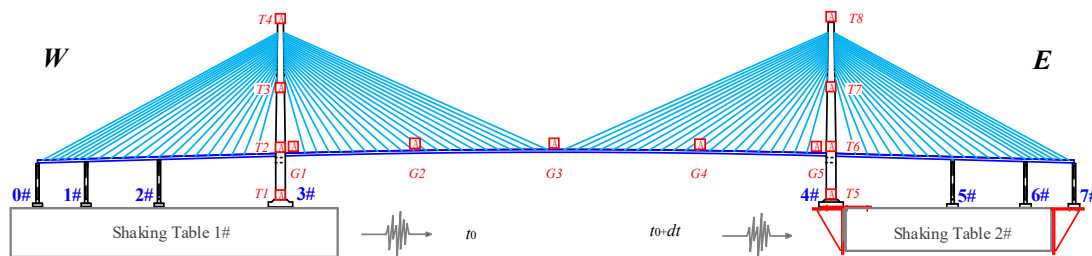
Figure 10. Schematic diagram of input excitations and sensors.

Besides, the seismic response of the CSB subjected to non-uniform excitation are studied. It should be noted that the non-uniform excitation in this paper only considers wave passage effects, while local site effects and incoherence effects are not considered. In the test, the wave passage effect is realized by the time delay (*dt*) between two tables, shown in Figure 10.

The delay time *dt* can be calculated by following formula:

$$dt = \frac{L}{v_{app}} \cdot S_t \qquad (1)$$

L stands for the distance of two points; V_{app} stands for the apparent wave velocity. In this paper, different V_{app} is studied, such as 480 m/s, 240 m/s and 120 m/s; S_t stands for the similitude ratios of time, that is 0.0707 in table 2. As the main span of the CSB is 680 m, delay time *dt* in the test is calculated as 0.1 s, 0.2 s and 0.4 s, listed in Table 4.

Table 4. The shake table test cases.

Test cases	Uniform Excitation		Non-Uniform Excitation					
	Case1	**Case2**	**Case3**	**Case4**	**Case5**	**Case6**	**Case7**	**Case8**
Exctation	ScEL	ScTCU	ScEL	ScEL	ScEL	ScTCU	ScTCU	ScTCU
delay time *(dt)*	0 s	0 s	0.1 s	0.2 s	0.4 s	0.1 s	0.2 s	0.4 s

As mentioned above, the ScEL and ScTCU are adopted as input motions for comparing the different seismic responses due to the NNF the PNF motion. Table 4 shows the shake table test cases.

4. Seismic Response of CSBs Under Uniform Excitations

4.1. Reproduction Validation for Uniform Excitations

Figure 11a shows the accelerations recorded on the shake tables under the uniform excitation of ScEL. It shows the longitudinal movement of both tables are in the same order. Figure 11b shows the acceleration Fourier amplitudes comparison of the two tables. The result indicates the identical Fourier amplitudes distribution of both tables. In the other test cases, similar result can be observed. Generally, the measured data shows shake table system of Fuzhou University has a good reproduction accuracy for earthquake motions.
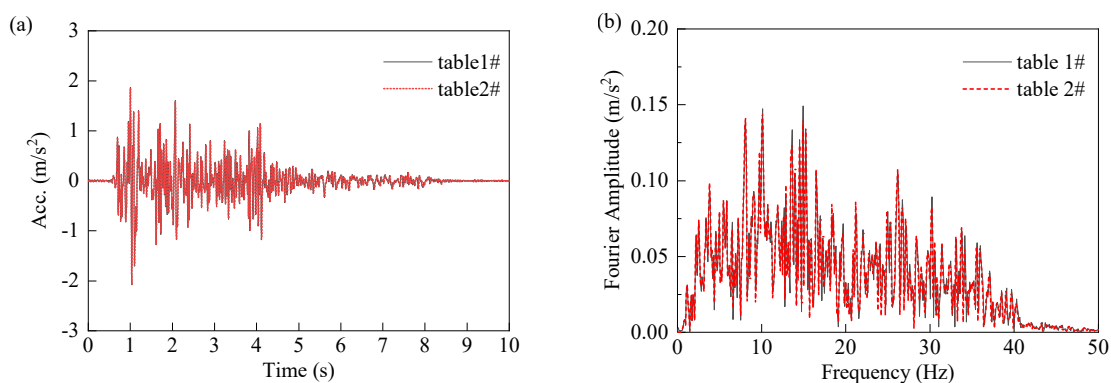
Figure 11. Measured accelerations of two tables subjected to uniform ScEL (Case1) (**a**) Time history (**b**) Fourier Amplitude.

4.2. Seismic Responses of Towers and Ppiers

4.2.1. Accelerations Responses

In the tests, the accelerometers are assembled on the key nodes of tower, such as on the lower-beam (T2), middle cross-beam (T3) and top node (T4). Figure 12a,b show the longitudinal acceleration responses of tower when subjected to uniform excitation of ScEL and ScTCU. As shown, the acceleration responses time histories of the different nodes are various. However, the peak time seem the same for all nodes. When subjected to NF excitations with same PGA (2.08 m/s²), maximal accelerations

subjected to NNF motion (ScEL) seems a little larger than the PNF motion (ScTCU). The phenomenon can be explained by the response Fourier spectrum, such as Figure 13a,b. As operation frequency limitation of the test system, the frequency range of 0~50 Hz are shown in the figures. It is obviously the energy of tower top node (T4) are mainly at 6.9 Hz, 13.8 Hz, 27 Hz, which are close to the frequencies of the 2nd, 4th, 5th modes. Among them, the 2nd mode dominate the acceleration response of tower top node. However, the response of mid cross beam (T3) has more energy than top node (T4). For f = 6.9 Hz, the peak amplitude is 0.05 m/s^2 for tower top node, while that is 0.15 m/s^2 for mid cross beam. In addition, there are an energy crest around 20 Hz, which is close to the frequency of the 5th mode. In the result, the acceleration response of tower mid cross beam is larger than top node. As shown in Figure 13b, the very similar phenomenon can be found in the tower response subjected to ScTCU.
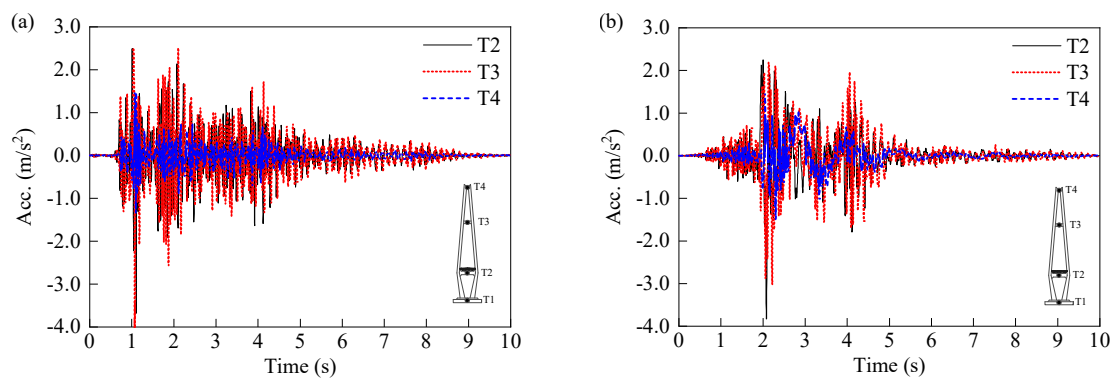

Figure 12. Accelerations time history of 3# tower (**a**) subjected to ScEL; (**b**) subjected to ScTCU.
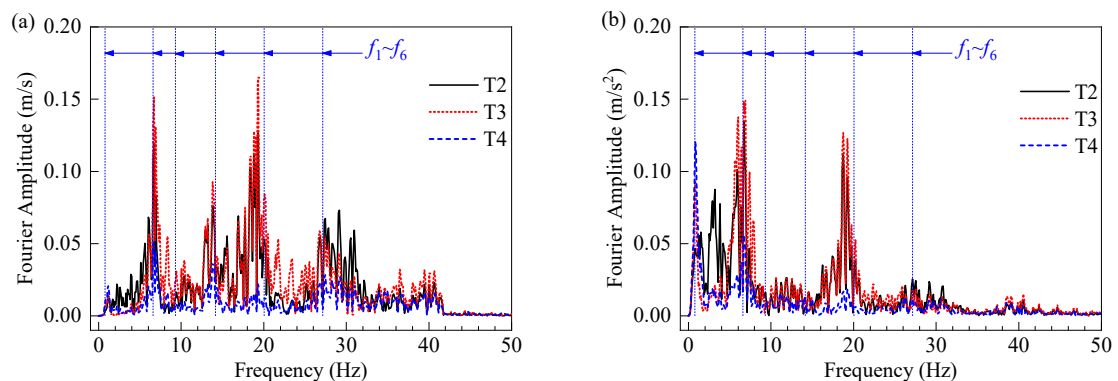

Figure 13. Accelerations Fourier amplitude of 3# tower (**a**) subjected to ScEL; (**b**) subjected to ScTCU.

Figure 14 shows the maximum tower acceleration distribution of the 3# tower and 4# tower. For the both towers, the maximum acceleration happens on middle cross beam (T3), rather than the tower top node (T4). The reason is the tower top node is effectively restricted by stayed-cables. In the result, the vibration on tower top node always smaller than mid cross beam under the longitudinal excitation. In general, from the point of view of longitudinal seismic response, the tower can be equivalent to a cantilever column with limited restriction on top node. When subjected to the ScEl, the acceleration responses seem a little larger than ScTCU. It should be noted that the acceleration for the same node of the two towers seems a little different. This may come from the manufacturing differences between the two towers or bearings.
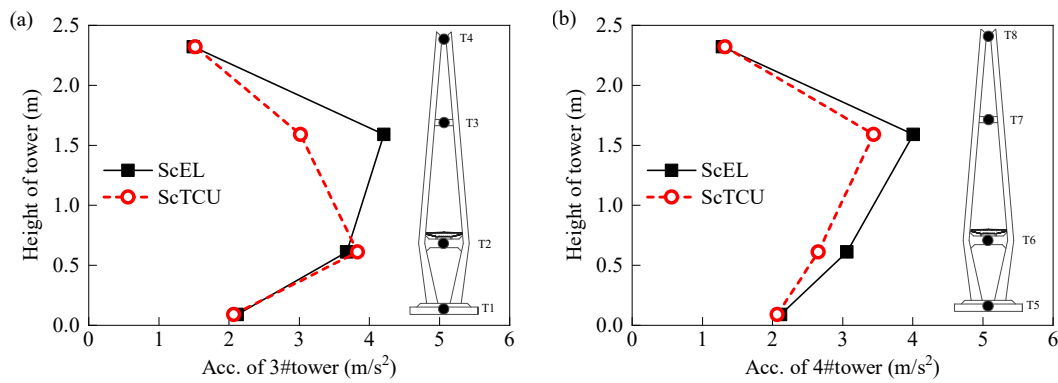
Figure 14. Maximum acceleration responses (**a**) 3# tower; (**b**) 4# tower.

4.2.2. Displacements Responses

Figure 15a,b show the absolute displacements of tower subjected to different excitations. As the towers are fixed on the shake table, the recorded movement on node T1 is approximately equal to the input excitation. It is obvious that the displacement of node T2 is similar to the node T1, while the node T3 and T4 are quite different to the base node. The similar phenomenon can be found in displacement responses subjected to the ScTCU in Figure 15b. The displacement response subjected to the ScTCU is significant larger than ScEL.
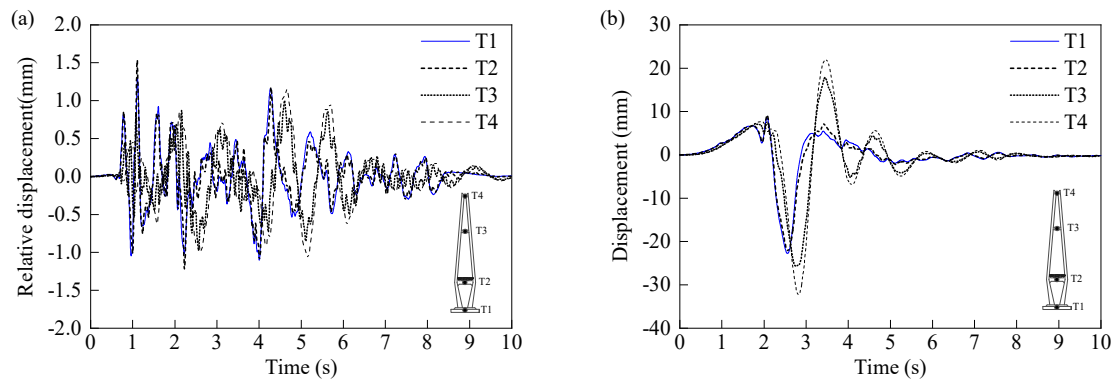

Figure 15. Displacement time history response of 3# tower (**a**) under ScEL; (**b**) under ScTCU.

Based on the response of the node T1, the relative displacement of tower key nodes can be calculated. Figure 16a,b shows the relative displacement response of tower subjected to different excitations. For the both NNF and PNF excitations, the relative displacements on the node T3 and node T4 are significant larger than the node T2. It can explain why the displacement of node T3 and node T4 are different from that of node T2 in the Figure 15.
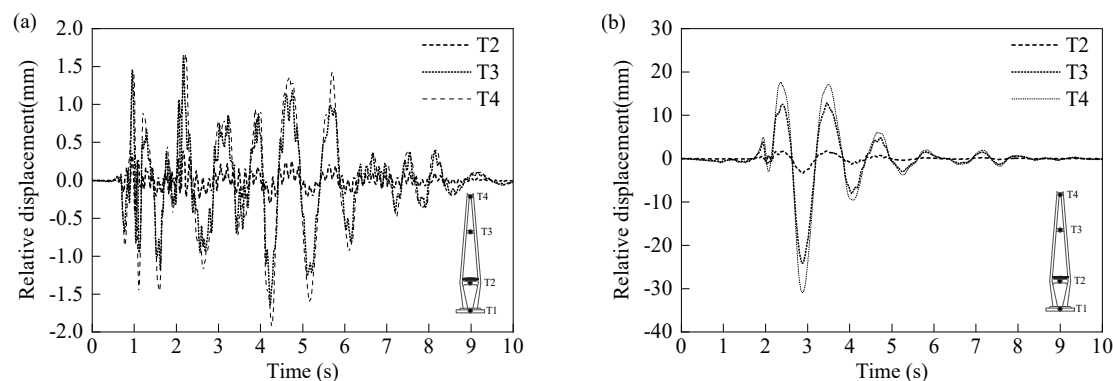

Figure 16. Relative displacement time history response of 3# tower (**a**) under ScEL; (**b**) under ScTCU.

For comparison, the maximum displacements and relative displacements of 3# tower are extracted and compared in Figure 17a,b. Both for displacement and relative displacement, the maximum values happen on the tower top node. However, the response values subjected to ScTCU are significant larger than ScEL. For the top node, the displacement and relative displacement subjected to ScTCU are 31.8 mm and 30.8 mm, while those are 1.6 mm 1.9 mm subjected to ScEL.
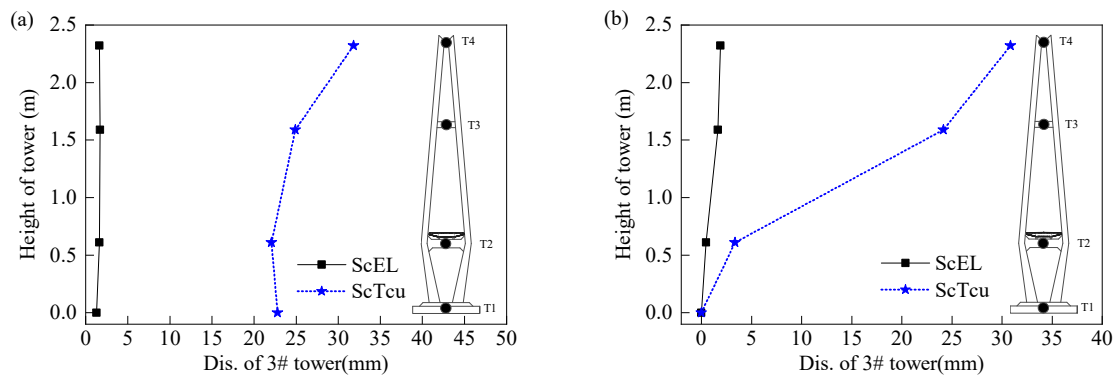

Figure 17. Maximum response of 3# tower for (**a**) displacement; (**b**) relative displacement.

It shows the velocity pulse has great impact on displacement and relative displacement responses, while have little effect on the acceleration response.

4.2.3. Strains and Bending Moment

The strain of 3# tower bottom section on both sides subjected to ScEL excitation are shown in Figure 18a. The strain responses on different sides (Sec T3-1E and Sec T3-1W) are changing nearly oppositely due to the bending effect. The maximum strain for Sec T3-1E is 24.1 $\mu\epsilon$. Based on strain response on the section edge, we can calculate the section bending moment, shown in Figure 18b. It shows the maximum bending moments of 3# tower is approach to 32 N·mm.
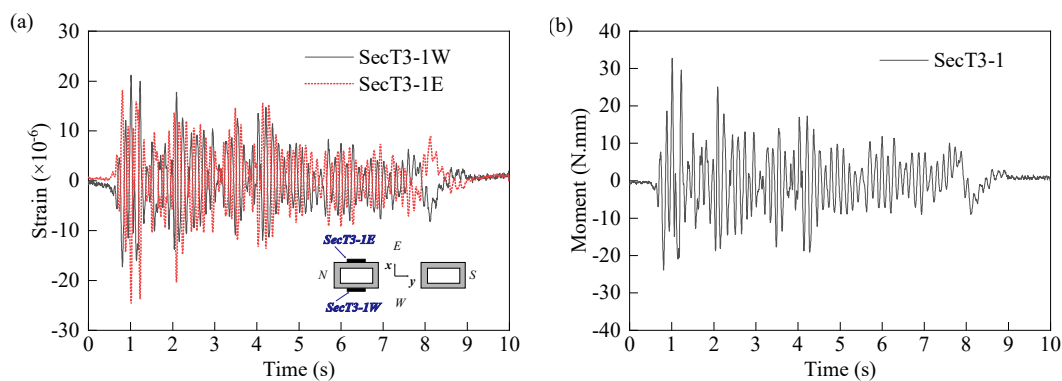

Figure 18. Seismic response of sectionT3-1 under ScEL (**a**) Strain response; (**b**) Bending moment.

Based on the above process, the maximum bending moments on other critical sections are calculated and shown in Figure 19a,b. For the sections above the girder, such as Sec T3-3, Sec T3-4, Sec T3-5, the bending moment are very small when subjected to the ScEL motions. However, the moments increase obviously from 11 N·mm to 32.8 N·mm for the tower below the lower cross-beam. On the contrary, when subjected to the ScTCU, the moments of section below the lower cross-beam also are large. For example, the moment reaches to 85 N·mm for secT3-3 subjected to ScTCU. Figure 19b shows the bending moments of the 4# tower. The similar conclusion can be drawn in the figure.
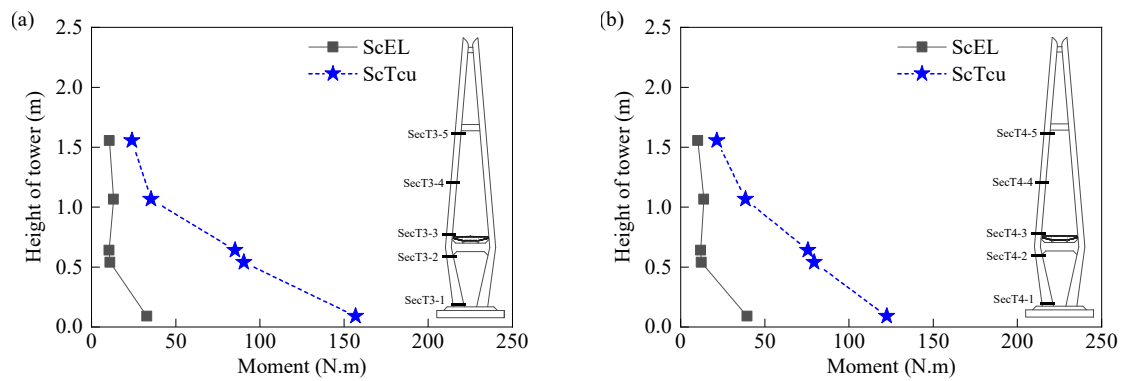
Figure 19. Moment of key sections along tower (**a**) 3# tower; (**b**) 4# tower.

Comparing the seismic response subjected to different NF motions, the bending motions subjected to the PNF (ScTCU) are significant larger than that of NNF (ScEL), about 2.98–4.50 times. This means the bending moments of tower are sensitive to the velocity pulse.

As we can see, the bottom sections is the most critical section for all piers. Table 5 shows the maximum bending moments of piers bottom sections. The largest responses happen on piers on the edge, such as 0# and 7#. For the 0# pier, bending moment subjected to ScEL and ScTCU are 10.23 N·mm and 13.84 N·mm respectively.

Table 5. Maximum bending moments on bottom sections of piers (unit: N·mm).

Components	0#Pier	1# Pier	2# Pier	5# Pier	6# Pier	7# Pier
under ScEL	10.23	10.01	9.98	10.14	10.23	10.23
under ScTCU	13.84	14.32	14.87	13.8	13.18	13.84

4.3. Seismic Responses of Girder

4.3.1. Longitudinal Responses

When the bridge is excited only in longitudinal direction, the longitudinal and vertical vibration are significant. Figure 20a shows the longitudinal acceleration of girder subjected to the ScEL and ScTCU. It is obviously the maximum acceleration subjected to ScTCU reaches 0.89 m/s^2, which is larger than 0.58 m/s^2 when subjected to ScEL. Figure 20b shows the Fourier amplitude of the longitudinal acceleration subjected to different type of NF motions. When subjected to the PNF (ScTCU), the Fourier amplitudes of the first and second order modes are significant larger than the NNF (ScEL). In the result, when subjected to ScTCU motion, the larger acceleration response of girder are recorded, shown in Figure 20a.
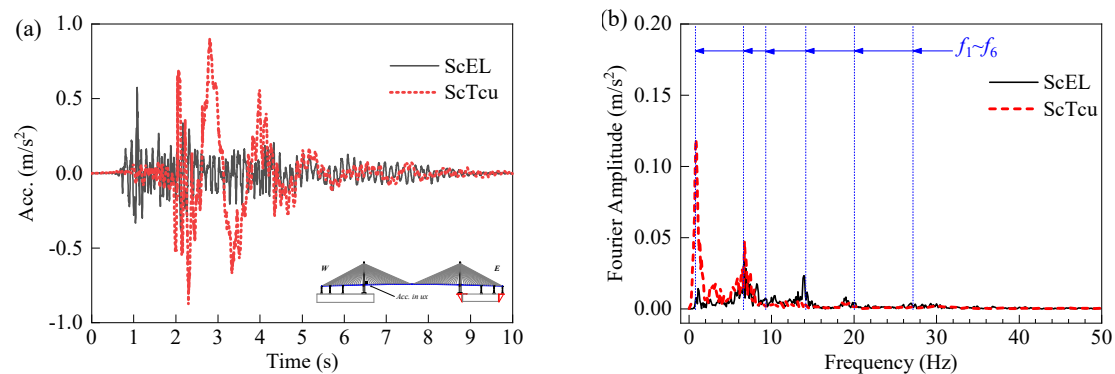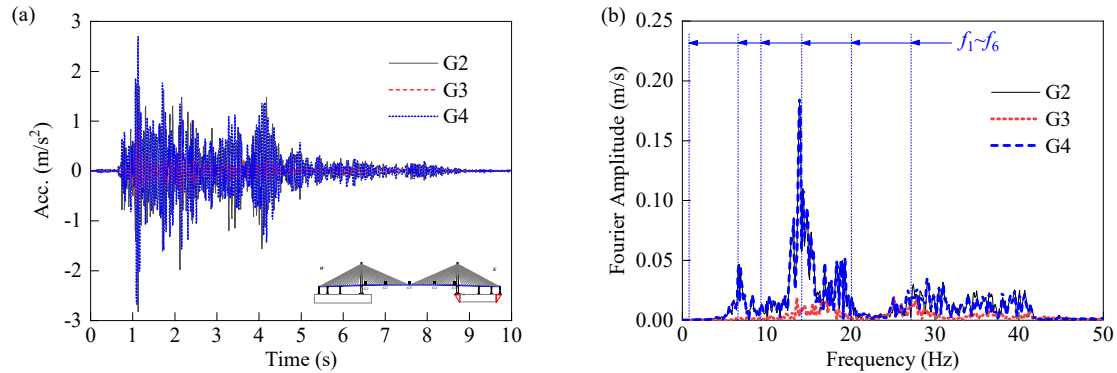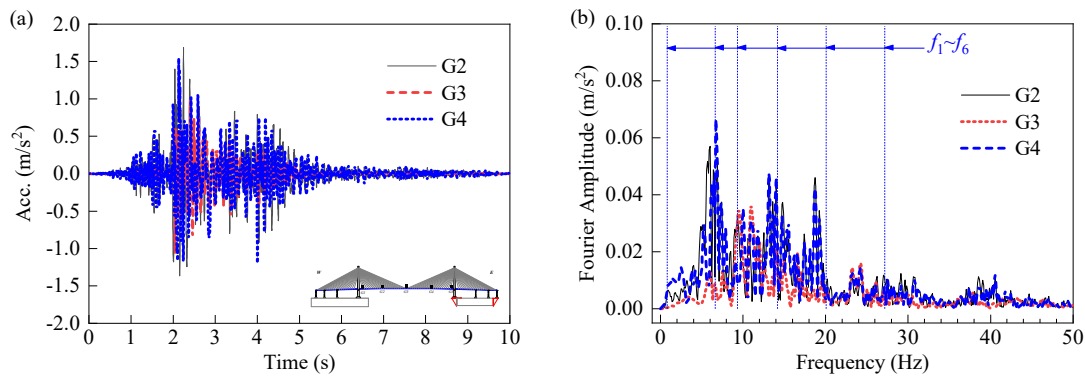

Figure 20. Longitudinal acceleration of girder. (**a**) Acceleration time histories; (**b**) Acceleration amplitude.

4.3.2. Vertical Response

The girder vertical vibration in different locations, such as 1/4 span (G2), 1/2 span (G3) and 3/4 span (G4) subjected to different type NF motions are shown in Figures 21 and 22.

Figure 21. Girder vertical acceleration under ScEL (**a**) Time history and (**b**) FFT.

Figure 22. Girder vertical accelerations under ScTCU (**a**) Time history and (**b**) FFT.

The maximum vertical acceleration of girder in 1/4 span, mid-span and 3/4 span are 2.88 m/s^2, 0.88 m/s^2, 2.70 m/s^2 separately. It is obviously that the vertical acceleration on the G2 and G4 are significant larger than node G3 on the mid-span when subjected to the ScEL. The amplitude spectrum of the accelerations time histories was analyzed by FFT method, shown in Figure 21b. The predominant frequency of the girder vertical vibration is about 13.9 Hz. which corresponds to the 4th vibration mode, shown in Figure 8d. The mode is a typical antisymmetric mode. In the result, the vibrations of the G2 and G4 are larger than the mid-span.

However, when subjected to the ScTCU, the vertical accelerations on the G2 and G4 are slight larger than the G3. The acceleration amplitude spectrums are shown in Figure 22b. We can find the contributions of the several modes are at a similar level, such as the 2nd, 3rd, 4th and 5th vibration mode. In the result, the peak accelerations on the G2, G3 and G4 are close.

For easier comparison, the peak vertical accelerations of different critical nodes of girder are shown in Figure 23a. The acceleration peak envelope curves subjected to both ground motions present "inverted W shape". However, the maximum accelerations subjected to the ScEL are significant larger than the ScTCU.

The displacements response of girder were computed from the accelerations by double integration and baseline correction. The maximum displacements of girder are drawn in Figure 23b. Similarly, both vertical displacement envelops are inverted 'W' shape, rather than 'U' shape. When subjected to the PNF motion (ScTCU), the maximum displacements are larger than the NNF motion.
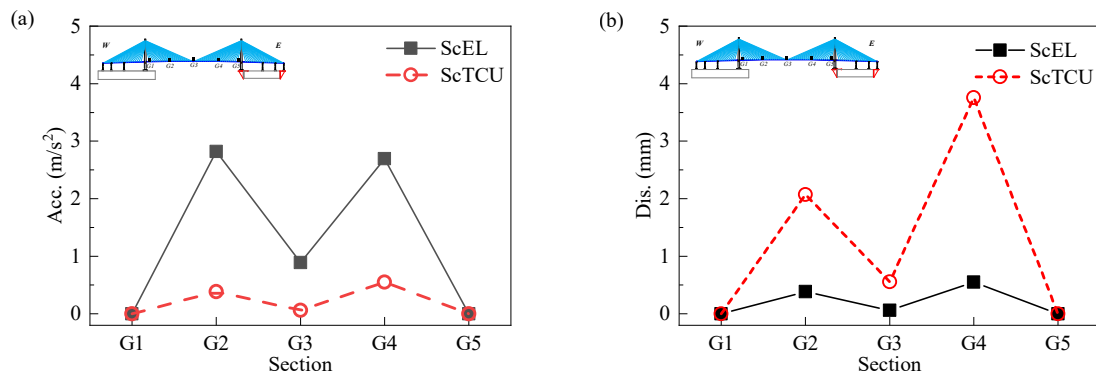
Figure 23. The maximum vertical response of girder for (**a**) acceleration and (**b**) displacement.

4.4. Seismic Responses of Bearing

Figure 24a shows the relative displacement between girder and tower. The maximum value subjected to ScTCU is 30 mm, which is far larger than ScEL. The amplitude spectrums of the relative displacement are shown in Figure 24b. It is dominated frequency is 0.79 Hz.
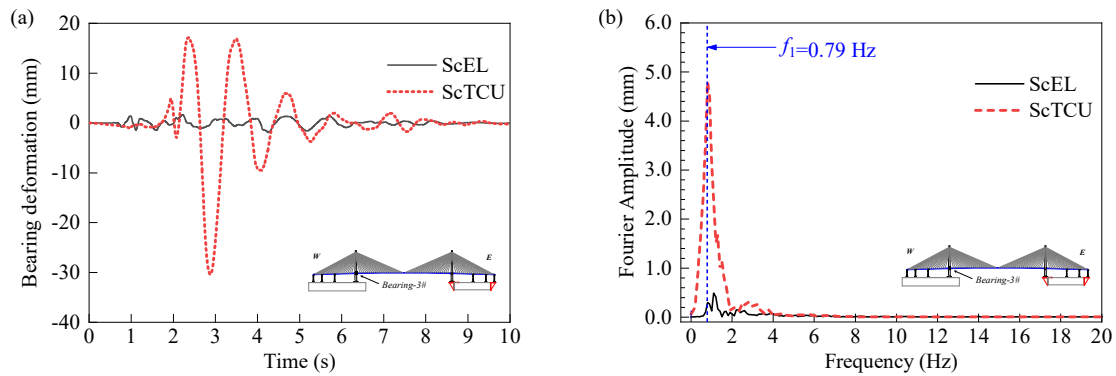

Figure 24. Longitudinal displacement of tower and girder on bearing connection (**a**) Bearing relative displacement (**b**) Fourier Amplitude.

4.5. Comparison of the Seismic Response

The magnitude responses of towers and girder subjected to both excitations are listed in Tables 6 and 7.

Table 6. The maximum longitudinal responses of 3# tower.

Excitation	Longitudinal Acceleration (m/s^2)			Longitudinal Displacement (mm)		
	T2-3#	T3-3#	T4-3#	T2-3#	T3-3#	T4-3#
ScEL	3.68	4.21	1.49	1.53	1.00	1.15
ScTCU	3.83	3.02	1.52	22.17	25.63	32.30

Table 7. The maximum vertical responses of girder.

Excitation	Vertical Acceleration (m/s^2)			Vertical Displacement (mm)		
	G2	G3	G4	G2	G3	G4
ScEL	2.82	0.89	2.69	0.38	0.06	0.55
ScTCU	1.69	1.06	1.54	2.07	0.56	3.76

It can be drawn from above tables that the accelerations amplitude of tower are very similar when subjected to both motions. The acceleration of girder subjected to ScTCU are smaller than ScEL. However, the displacement of both tower and girder subjected to ScTCU are great larger than ScEL.

The acceleration time histories and Fourier amplitudes are shown in Figures 12, 13, 21 and 22. From the acceleration Fourier amplitudes, the accelerations of both tower and girder are contribution by several different modes. Therefore, the acceleration responses are mainly determined by the several vibration modes of CSB and energy distribution of ground motions. From Figure 9b, the ScTCU has advantage in low frequency band, while the ScEL has more energy on the frequency band of [10 Hz, 30 Hz]. In the result, the acceleration responses subjected to both excitation are similar.

On the other hand, the displacement responses subjected to the ScTCU are significant larger than ScEL. There are two mainly reasons: the first is the quite different PGD of both input motions. Although the PGA of both motions are the same, the PGV and PGD are very different, shown in Figure 9c,d. The PGD of ScEL and ScTCU are 1.3 mm and 22.8 mm, respectively. The other reason is the energy of ScTCU concentrates in the low frequency band, shown in Figure 9b. Meanwhile, the displacement response of CSB are mainly contributed by the long period component, shown in Figure 15a,b. In summary, the displacement response induced by the ScTCU are significant larger than the ScEL.

5. Seismic Responses of CSBs Under Non-Uniform Excitations

5.1. Non-Uniform Test Cases

In these tests, only the wave passage effect, which is caused by the different arrival times of the same ground motions, is considered. Therefore, for the non-uniform test cases, the excitations of two tables are the same, however, the excitation on the 2# table is delayed by dt, shown in Figure 10. The tested non-uniform cases are shown in Table 4.

Taking the non-uniform ScEL with dt = 0.1 s (Case3 in Table 4) for example, the recorded input longitudinal displacement of two shake tables are shown in Figure 25a. As the figure shows, the displacement of two tables almost the same, except a time delay of 0.1 s. It shows the multi-tables system have reproduced the wave passages excitation accurately with the expectant delay time.
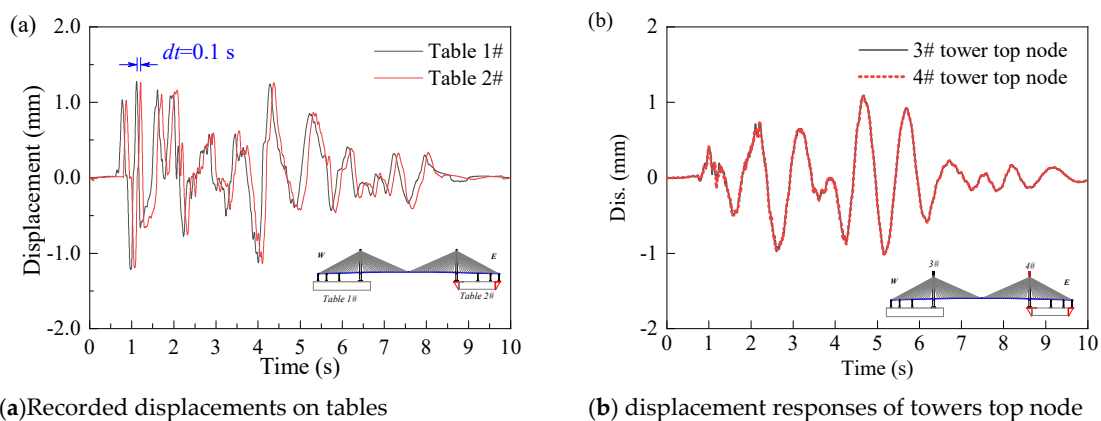

(**a**)Recorded displacements on tables　　　　　(**b**) displacement responses of towers top node

Figure 25. Responses recorded under time delayed excitation of ScEL (dt = 0.1 s).

When subjected to the non-uniform ScEL with dt = 0.1 s, the displacements of tower top nodes are shown in Figure 25b. The test results shows the displacement of two towers seems consistent as effective restraint of stayed-cables.

5.2. Seismic Responses Subjected to the Non-Uniform Excitations

During the tests, six non-uniform cases were carried out, shown in Table 4. The delay times are 0.1, 0.2 and 0.4 s, respectively. Based on the measured accelerations time history, we can get the displacement time histories through direct integration and baseline correction. The relative displacement is the displacement to tower base, which can be calculated by displacement subtracting in time history. The tower relative displacements envelopes are shown in Figure 26a,b. When subjected to the uniform excitations, the relative displacements on both tower tope nodes are consistent. While the tower relative displacements are quite different when subjected to the time delayed excitations. For non-uniform cases with different delay time (*dt*), the responses also seems quite different. However, the relative displacement responses excited by different *dt* seems to have no obvious rules to follow.
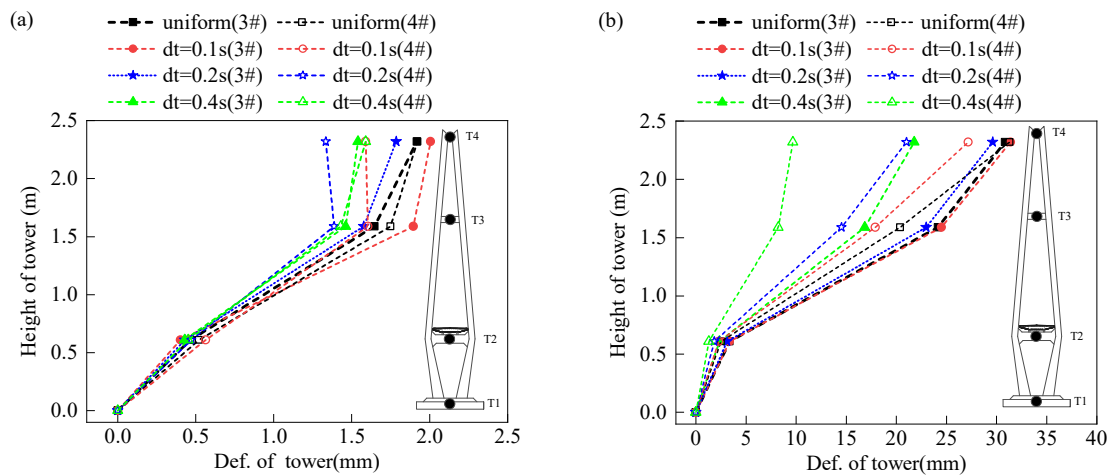

Figure 26. Relative displacements response of towers subjected to (**a**) ScEL (**b**) ScTCU.

Figure 27a,b show the maximum vertical deformation of girder subjected to different non-uniform excitations. As shown in Figure 27a, when non-uniform excited by ScEL, the vertical deformation on the mid-span (G3) are larger than uniform excitation. The reason is the symmetrical modes, such as the 4th, 6th modes, are more seriously excited by the non-uniform excitations. Secondly, comparing the non-uniform cases with different *dt*, the deformation on the G4 is more sensitive than G2. It means wave passage effect has a greater impact on the nodes located farther away, such as G4, when the excitation is propagating from G1 to G5.
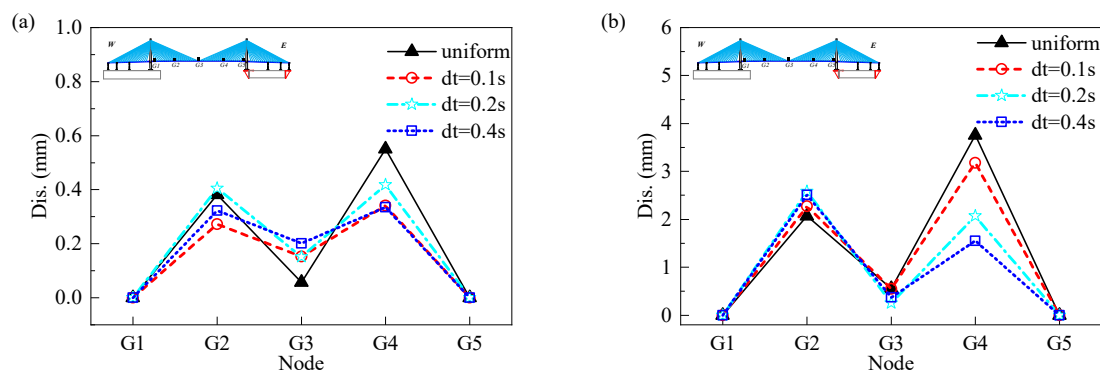

Figure 27. The maximum vertical deformation of girder subjected to (**a**) ScEL; (**b**) ScTCU.

Figure 27b shows the girder deformation when subjected to the PNF ground motions (ScTCU). Similar to the previous Figure, the deformation on the node G4 is significant various for different non-uniform cases. In order to explain this rule more clearly, Figure 28 shows the deformation response time history diagrams subjected to different non-uniform cases. For the uniform case, the maximum deformation on the node G4 is larger than the node G2. However, for non-uniform with $dt = 0.4$ s, the maximum deformation on node G4 is significant reduced. Further, the peaking time is also different to the uniform cases. In contrast, the deformation response of node G2 is less different for different non-uniform cases.
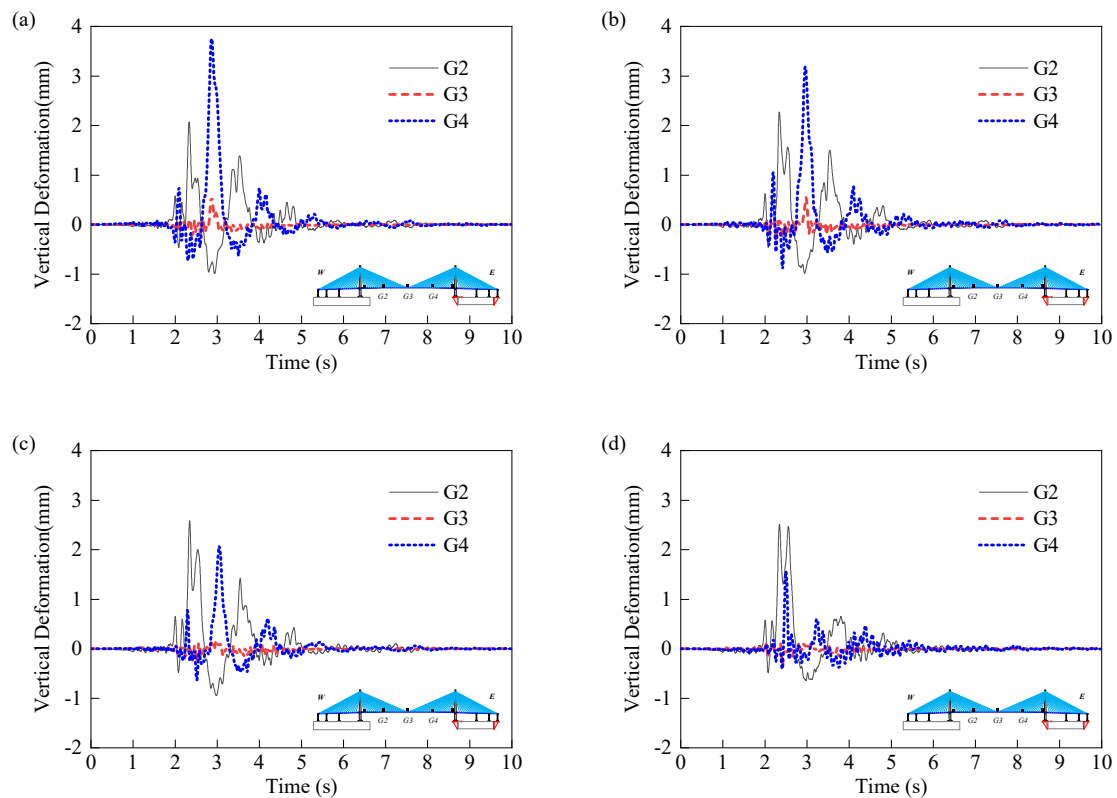
Figure 28. The girder vertical deformation time history subjected to ScTCU with (**a**) uniform; (**b**) $dt = 0.1$ s; (**c**) $dt = 0.2$ s; (**d**) $dt = 0.4$ s.

6. Conclusions

To evaluate the seismic response of CSBs subjected to NF ground motions, a scaled CSB was designed and fabricated. Two NNF and PNF motions were selected as the input excitations. The shake table test of scaled CSB subjected to uniform and non-uniform excitations were carried out. The following conclusions can be made based on the test results:

(1) The first six modes and the corresponding frequencies of the scaled CSB were identified using the SSI method. The fundamental mode shows as girder and tower longitudinal vibration with a frequency of 0.79 Hz. The 2nd mode shows as girder vertical antisymmetric vibration combing tower longitudinal bending with a frequency of 6.61 Hz. In the first six in-plane modes, the 2nd, 4th and 6th modes are antisymmetric, while the 1st, 3rd and 5th modes are symmetric.

(2) The maximum displacement of the tower occurs on the tower top node, the maximum acceleration response of the tower occurs on the middle cross beam, and the maximum bending moment of the tower occurs on the bottom section

(3) The deformation of the tower and girder subjected to uniform excitation is not always larger than that subjected to non-uniform excitation, and therefore the non-uniform case should be considered in the seismic design of CSBs.

References

1. Xu, Y.; Hu, S. Seismic design of high-rise towers for cable-stayed bridges under strong earthquakes. *Front. Arch. Civ. Eng. China* **2011**, *5*, 451–461. [CrossRef]

2. Soneji, B.; Jangid, R. Passive hybrid systems for earthquake protection of cable-stayed bridge. *Eng. Struct.* **2007**, *29*, 57–70. [CrossRef]

3. Loh, C.-H.; Liao, W.-I.; Chai, J.-F. Effect of near-fault earthquake on bridges: Lessons learned from Chi-Chi earthquake. *Earthq. Eng. Struct. Vib.* **2001**, *1*, 86–93. [CrossRef]

4. Xu, Y.; Duan, X.; Li, J. Seismic design strategy of cable stayed bridges subjected to strong ground motion. *Struct. Eng. Mech.* **2012**, *51*, 909–921. [CrossRef]

5. Yi, J.; Li, J. Effect of Seismic-Induced bearing uplift of a Cable-Stayed bridge. *J. Bridge Eng.* **2019**, *24*, 4018125. [CrossRef]

6. Fang, Z.; Zhang, C.; Chen, Y.; Zheng, Z.; Xu, L. Research on the shaking table test of three towers cable-stayed bridge based on three shaking table system. *China Civ. Eng.* **2012**, *45*, 25–29. (In Chinese)

7. Yadi, S.; Suhendro, B.; Priyosulistyo, H.; Aminullah, A. Shake table test of floating cable-stayed bridge under earthquake excitation during construction with balanced cantilever method. *Int. J. Civ. Eng. Technol.* **2018**, *9*, 2063–2081.

8. Xu, L.; Zhang, H.; Gao, J.; Zhang, C. Longitudinal seismic responses of a cable-stayed bridge based on shaking table tests of a half-bridge scale model. *Adv. Struct. Eng.* **2018**, 1–13. [CrossRef]

9. Xie, W.; Sun, L. Experimental and numerical verification on effects of inelastic tower links on transverse seismic response of tower of bridge full model. *Eng. Struct.* **2019**, *182*, 344–362. [CrossRef]

10. Yadi, S.; Suhendro, B.; Priyosulistyo, H.; Aminullah, A. Dynamic response of long-span bridges subjected to nonuniform excitation: A state-of-the-art review. *Matec. Web. Conf.* **2019**, *258*, 5017. [CrossRef]

11. Shiravand, M.R.; Parvanehro, P. Spatial variation of seismic ground motion effects on nonlinear responses of cable stayed bridges considering different soil types. *Soil Dyn. Earthq. Eng.* **2019**, *119*, 104–117. [CrossRef]

12. Li, S.; Zhang, F.; Wang, J.-Q.; Alam, M.S.; Zhang, J. Seismic responses of super-span cable-stayed bridges induced by ground motions in different sites relative to fault rupture considering soil-structure interaction. *Soil Dyn. Earthq. Eng.* **2017**, *101*, 295–310. [CrossRef]

13. Liang, F.; Jia, Y.; Sun, L.; Xie, W.; Chen, H. Seismic response of pile groups supporting long-span cable-stayed bridge subjected to multi-support excitations. *Soil Dyn. Earthq. Eng.* **2017**, *101*, 182–203. [CrossRef]

14. Jia, H.; Lan, X.; Zheng, S.; Li, L.; Liu, C. Assessment on required separation length between adjacent bridge segments to avoid pounding. *Soil Dyn. Earthq. Eng.* **2019**, *120*, 398–407. [CrossRef]

15. Kojima, K.; Takewaki, I. Critical earthquake response of elastic-plastic structures under Near-Fault ground motions (Part 2: Forward-Directivity input). *Front. Built Environ.* **2015**, *1*, 1–13. [CrossRef]

16. Ardakani, S.; Saiidi, M.S. Simple method to estimate residual displacement in concrete bridge columns under near-fault earthquake motions. *Eng. Struct.* **2018**, *176*, 208–219. [CrossRef]

17. Adanur, S.; Altunişik, A.C.; Bayraktar, A.; Akköse, M. Comparison of near-fault and far-fault ground motion effects on geometrically nonlinear earthquake behavior of suspension bridges. *Nat. Hazards* **2012**, *64*, 593–614. [CrossRef]

18. Yang, D.; Zhao, Y.; Li, G. Influence analysis of motion characteristics of near-fault ground motions on seismic responses of long-period structures. *J. Disaster Prev. Mitig. Eng.* **2007**, *27*, 133–140. (In Chinese)

19. Zhou, L.; Wang, X.; Ye, A. Effectiveness evaluation and optimal design of nonlinear viscous dampers for inelastic structures under pulse-type ground motions. *Earthq. Eng. Struct. Dyn.* **2018**, *47*, 2802–2820.

20. Zhou, L.; Wang, X.; Ye, A. Shake table test on transverse steel damper seismic system for long span cable-stayed bridges. *Eng. Struct.* **2019**, *179*, 106–119. [CrossRef]

21. Lesgidis, N.; Kwon, O.-S.; Sextos, A. A time-domain seismic SSI analysis method for inelastic bridge structures through the use of a frequency-dependent lumped parameter model. *Earthq. Eng. Struct. Dyn.* **2015**, *44*, 2137–2156. [CrossRef]

22. Shahi, S.K.; Baker, J.W. An efficient algorithm to identify Strong-Velocity pulses in multicomponent ground motions. *Bull. Seismol. Soc. Am.* **2014**, *104*, 2456–2466. [CrossRef]

23. Ancheta, T.; Darragh, R.; Stewart, J.; Silva, W.J.; Chiou, B.S.J.; Wooddell, K.E.; Graves, R.W.; Kottke, A.R.; Boore, D.M.; Kishida, T.; et al. *PEER NGA-West2 Database*; Technical Report 2013/03; Pacific Earthquake Engineering Research Center: Berkeley, CA, USA, 2013.

24. Okamoto, Y.; Nakamura, S. Static and seismic studies on steel/concrete hybrid towers for multi-span cable-stayed bridges. *J. Constr. Steel Res.* **2011**, *67*, 203–210. [CrossRef]

25. Martinez-Rodrigo, M.D.; Filiatrault, A. A case study on the application of passive control and seismic isolation techniques to cable-stayed bridges: A comparative investigation through non-linear dynamic analyses. *Eng. Struct.* **2015**, *99*, 232–252. [CrossRef]